*Journal of The Electrochemical Society*, **153** (1) A75-A80 (2006)
0013-4651/2005/153(1)/A75/6/$20.00 © The Electrochemical Society, Inc.



# Investigation on Capacitance Mechanisms of $Fe_3O_4$ Electrochemical Capacitors

**Shih-Yu Wang, Kuo-Chuan Ho,* Shin-Liang Kuo, and Nae-Lih Wu*,z**

*Department of Chemical Engineering, National Taiwan University, Taipei 106, Taiwan, Republic of China*

The capacitance mechanisms of magnetite ($Fe_3O_4$) electrochemical capacitor in $Na_2SO_3$, $Na_2SO_4$, and KOH aqueous solutions have been investigated by electrochemical quartz-crystal microbalance analysis, along with cyclic voltammetry and X-ray photoelectron spectroscopy. The oxide thin-film electrode was prepared by an electroplating method, and exhibits a capacitance of ~170, 25, and 3 F/g in 1.0 M $Na_2SO_3$(aq), $Na_2SO_4$(aq), and KOH(aq), respectively. Strong specific adsorption of the anion species was evidenced in all solutions. Experimental results indicate that, in $Na_2SO_3$(aq), the capacitive current of magnetite electrode originates from the combination of electric double-layer capacitance (EDLC) and the pseudocapacitance that involves successive reduction of the specifically adsorbed sulfite anions, from $SO_3^{2-}$ through, e.g., $S^{2-}$, and vice versa. In $Na_2SO_4$(aq), the current is due entirely to EDLC. Furthermore, due to the specific adsorption behavior, magnetite exhibits high EDLC, >30 $\mu F/cm^2$, in both $Na_2SO_3$ and $Na_2SO_4$ solutions. The lowest capacitance of magnetite was observed in KOH, which is attributed to the formation of an insulating layer on the magnetite surface.
 [DOI: 10.1149/1.2131820] 

Manuscript submitted April 29, 2005; revised manuscript received September 6, 2005.
Available electronically November 28, 2005.

Electrical double-layer capacitance (EDLC) arises from the potential dependence of the surface density of charges stored electrostatically (i.e., nonfaradaically) at the interfaces of capacitor electrodes.[1-4] EDLC electrochemical capacitors are complemented by capacitors based on the so-called pseudocapacitance, which involves faradaic reactions but behaves like a capacitor rather than a galvanic cell.[5-15] While EDLC typically has a specific capacitance in the order of 10 $\mu F/cm^2$ of true surface area of the electrode material, pseudocapacitance often has a value that is 10 to 100 times greater.

The most widely studied pseudocapacitive material is hydrous $RuO_2$.[5-9] The pseudocapacitance of this material is known to arise from successive multielectron transfer at Ru cation sites, from, e.g., $Ru^{2+}$ to $Ru^{3+}$ and then to $Ru^{4+}$, balanced by conversion of the $OH^-$ site to the $O^{2-}$ sites in the oxide structure by proton transfer. There is a continuously variable degree of oxidation/reduction, leading to the capacitor behavior. Because $RuO_2$ is very expensive, searching for cheaper pseudocapacitive electrode materials has been a major subject in the research on electrochemical capacitors. Goodenough et al.[10,11] reported in 1999 the observation of pseudocapacitance on hydrous $MnO_2$. Its mechanism was suggested to involve multielectron transfer at Mn cation sites, balanced by intercalation/extraction of cations within the oxide structure.

An aqueous $Fe_3O_4$ (magnetite) electrochemical capacitor is another emerging inexpensive system.[12-16] Large capacitances have been reported in alkali sulfites and sulfate solutions. In particular, the capacitance of the oxide was found to be sensitive to the anion species but not to either alkaline cations or electrolyte pH ($\leqslant$11). These behaviors suggest a capacitance mechanism that is different from that of either $RuO_2$ or $MnO_2$. Preliminary investigation,[13] simply based on the dependence of the rest potential on electrolyte concentration, has failed to conclude the mechanism. In this work, the capacitance mechanisms of a magnetite electrode in $Na_2SO_3$, $Na_2SO_4$, and KOH aqueous solutions have been established, in particular, by electrochemical quartz-crystal microbalance (EQCM) analysis and X-ray photoelectron spectroscopy (XPS), along with other electrochemical characterizations.

## Experimental

For the EQCM analysis, nanocrystalline magnetite film was electroplated onto the EQCM (gold) working electrode under a constant potential of 0.6 V vs Ag/AgCl. [All the potentials reported here are referenced to a commercial reference electrode, Ag/AgCl/saturated KCl(aq), from EG&G, which is 0.197 V vs normal hydrogen electrode (NHE) at 25°C.] The electroplating solution was prepared by mixing 50 mL of 1.0 M $FeCl_2$ and 200 mL of 1.6 M $CH_3COONH_4$ along with sufficient NaOH to adjust the solution pH to 9.5. The solution was de-aerated by bubbling $N_2$, and the plating did not start until the solution turned dark greenish. The structure of the oxide film was characterized by X-ray diffraction (XRD; Philips/X'pert diffractometer with Cu K$\alpha$ radiation), and the amount of oxide film was determined by completely dissolving the film in HCl and then measuring the concentration of Fe ions by using Induction Coupled Plasma (ICP; Perkin Elmer/ICP Optima 3000) element analysis. The morphology of the oxide film was characterized by scanning electron microscopy (LEO 1530). XPS analysis was carried out on a spectrometer (MT 500, VG Microtech) equipped with a Mg (K$\alpha$) X-ray source. To be prepared for the XPS analysis, the electrodes were first dried by being sandwiched between two filter papers to remove a major portion of the residue solution, and then further dried and stored under vacuum at room temperature before being sent to an XPS chamber in 8 h.

The EQCM (CH Instruments, Model CHI 440) measures the frequency difference between the working crystal and the reference crystal. The resonant frequency of the fundamental mode of the reference crystal ($f_o$) is 8.0 MHz. The correlation between mass change ($\Delta m$) and frequency variation ($\Delta f$) was calculated based on the Sauerbrey equation

$$\Delta f = -2f_o^2 \Delta m / A(\mu\rho)^{0.5} \quad [1]$$

where $\Delta f$ is in Hz, $\Delta m$ is in g, $A$ is the area of the gold working electrode (0.196 $cm^2$), $\mu$ is the shear parameter of quartz ($2.947 \times 10^{11}$ g/cm $s^2$), and $\rho$ is the density of quartz (2.684 $g/cm^3$). Substitution of all the parameters into Eq. 1 shows that a frequency variation of +1 Hz corresponds to a mass change of −1.36 ng. In a typical run, the potential of the oxide-coated working electrode was cycled at a constant scan rate in a three-electrode configuration which comprises a gold counter electrode and an Ag/AgCl reference electrode, and the current and quartz frequency were simultaneously recorded. Three aqueous electrolyte solutions have been employed for the study, including 1.0 M $Na_2SO_3$, 1.0 M $Na_2SO_4$, and 1.0 M KOH. The solutions were de-aerated before being introduced into the EQCM cell.

## Results and Discussion

The deposited oxide film appeared black, and XRD showed it to be single-phased magnetite. The oxide film exhibited granular morphology with high porosity (Fig. 1). Calculation using Scherrer's

* Electrochemical Society Active Member.
z E-mail: nlw001@ccms.ntu.edu.tw

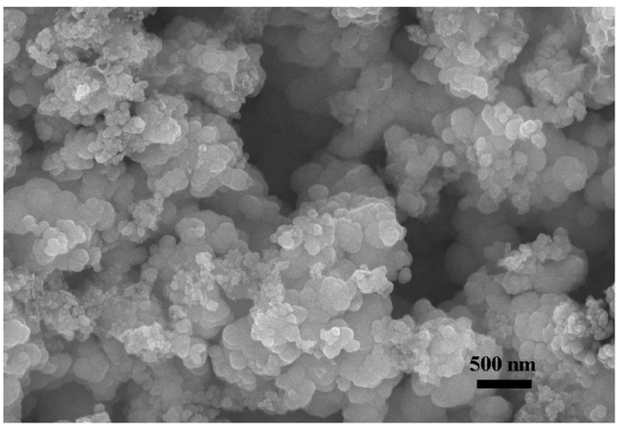


**Figure 1.** SEM micrograph of the magnetite thin-film electrode.

equation based on the full width at half-maximum intensity of the (311) reflection of $Fe_3O_4$ gave an average crystallite size of 12 nm. The total mass of the oxide film was 7.70 μg.

*Static EQCM study*.— In the first part of the EQCM study, mass variations of the magnetite thin-film electrode arising from immersion in the electrolyte solutions were measured without imposing potential scan. This "static" protocol was meant to determine the extent of specific adsorption, if any, on the oxide film. Initially, after being dried and subsequently loaded onto the electrode stage of the EQCM cell, the oxide electrode was allowed to equilibrate in air. As shown in Fig. 2, the frequency, and hence the electrode mass, remained rather constant during this period of time. Then, a drop of deionized water that was just sufficient to immerse the entire working electrode was added. Upon introduction of the water drop, the frequency decreased promptly and drastically to a minimum and then rose slightly to reach a plateau (solid line, Fig. 2). More drops were then successively added. It was found that, with each drop introduced, the frequency responded first with a small dip and then rose back to the same level again.

The same procedures described above were repeated except that each time a different electrolyte solution was used. As shown in Fig. 2, in all cases, the frequency responded in a qualitatively similar fashion to that described for deionized water, but there were significant differences in the final equilibrium frequency. Deionized water gave the highest equilibrium frequency, while all the other electrolyte solutions resulted in lower equilibrium frequencies. That is, the oxide film is "heavier" in electrolyte solutions than in deionized

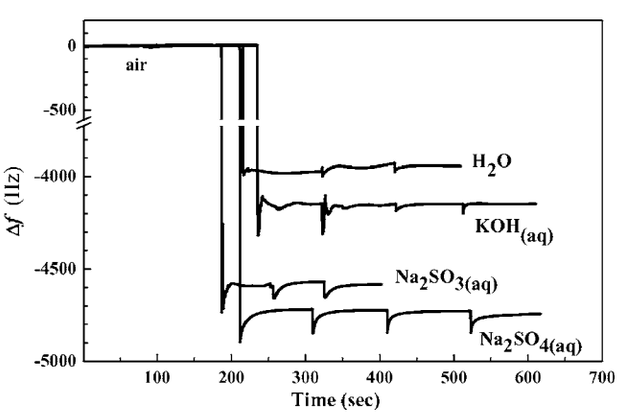


**Figure 2.** Frequency variation $\Delta f$ of EQCM upon introduction of electrolyte solution. The dips mark the moments when drops of electrolyte solution are introduced.

**Table I. Initial mass gains in various electrolytes measured by an EQCM.**

| Electrolyte | $\Delta f$ (Hz) | $\Delta m$ (ng) | Equivalent formula weight (EFW) of anion (g/mol) | $\Delta m$/EFW (nmol) |
|---|---|---|---|---|
| $Na_2SO_3$ | −636 | +852 | 40 ($SO_3^{2-}$) | 21.3 |
| $Na_2SO_4$ | −785 | +1052 | 48 ($SO_4^{2-}$) | 21.9 |
| KOH | −208 | +279 | 17 ($OH^-$) | 16.4 |

water. The differences in "apparent mass" are believed to arise mainly from specific adsorption of ions, which varies from one electrolyte solution to another. The extra mass gains of the oxide film, as referenced to that in deionized water, for different electrolyte solutions are summarized in Table I.

It was noticed that, if the extra mass gains in $Na_2SO_3$ and $Na_2SO_4$ solutions were divided, respectively, by the equivalent formula weights (EFWs) of the corresponding electrolyte anions, namely sulfite ($SO_3^{2-}$) and sulfate ($SO_4^{2-}$), almost the same equivalent mole numbers were obtained for both electrolytes. A reasonable interpretation is that the extra mass gains resulted mainly from the specific adsorption of the anion species and that they basically adsorbed at the same type of surface sites of the oxide. In the KOH solution, a less equivalent amount of adsorbed $OH^-$ was observed as compared with sulfite and sulfate anions in their electrolyte solutions. It is well known that specific adsorption requires loss of the hydration sheath of the adsorbed ions, at least toward the substrate side, and therefore larger ions are more easily specifically adsorbed than the smaller, heavily hydrated ions.[4] Accordingly, it is not surprising to find out that either the sulfite or the sulfate anion would play a much more important role in specific adsorption than sodium cation in the present electrolyte solutions. The same principle can also be applied to explain, at least in part, why $OH^-$ adsorbed with a less amount than either the sulfite or sulfate anion did. The surface Fe ions are not fully coordinated by lattice oxygen atoms, and thus are the most likely adsorption sites for the anions.

*Dynamic EQCM study*.— In the second part of the EQCM study, mass variations, along with the induced currents, of the oxide electrode at the potential scan rate of 2 mV/s were recorded. Figure 3 gives the current-vs-potential (*I-E*) plots recorded for the three different electrolyte solutions employed. A plot acquired with the blank gold electrode (i.e., without the magnetite film) is also shown for comparison. For $Na_2SO_3$(aq), the plot exhibits a nonrectangular profile containing broad humps and peaks, indicative of some sort of redox reactions. Because of the nonrectangular current profile, an average capacitance $C_{avg}$ is calculated from

$$C_{avg} = \Delta Q/\Delta E = \left[\int IdE/(dE/dt)\right] \Big/ \Delta E \qquad [2]$$

where $\Delta Q$ is the total amount of charge accumulated over a potential window $\Delta E$, $I$ is the current, and $t$ is the time. Calculation between −0.2 and −0.7 V (to disregard the transition regions upon the reversal of potential scan) gives a $C_{avg}$ of 174(±2) F/g (i.e., 172 and 176 F/g for the reductive and oxidative scans, respectively). It is much greater than that for either $Na_sSO_4$(aq) or KOH(aq), which exhibits a $C_{avg}$ of 25 and 3 F/g, respectively. An irreversible oxidation process can be noticed in KOH(aq) during the oxidative scan near the high-potential end (inset in Fig. 3).

Figure 4 shows a typical pair of the *I-E* and *m-E* (mass-vs-potential) plots for $Na_2SO_3$(aq). The zero points of the *y*-axis in all the *m-E* plots described hereafter were set at the onset of the reductive potential scan (point A). As marked in the figures, the loops start from point A, where the potential scan just reverses from the oxidative direction to the reductive one. The *m-E* plot shows first a slight mass increase, by 12 ng, until nearly −0.35 V (point B), and then a

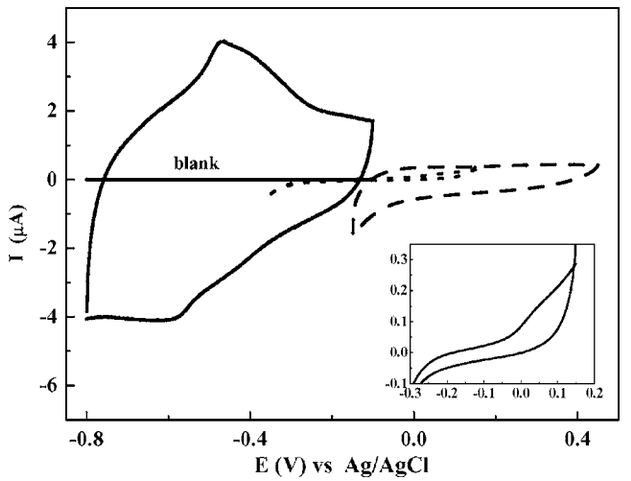


**Figure 3.** Cyclic voltammograms for magnetite electrode in different electrolyte solutions, including 1.0 M $Na_2SO_3$(aq) (solid line), 1.0 M $Na_2SO_4$(aq) (dashed line), and 1.0 M KOH(aq) (dotted line). The inset shows an enlarged portion of the plot in KOH. The line marked as "blank" is acquired with the gold electrode without the oxide layer in 1.0 M $Na_2SO_3$(aq). The potential scan rate is 2 mV/s.

monotonic mass reduction, by −69 ng, until −0.8 V (point C). Upon the reversal of potential scan, the mass shows a slight decrease until nearly −0.55 V (point D). This is then followed by a rapid mass increase until the upper potential limit of the oxidative scan. Thus, the *m-E* plot obtained for $Na_2SO_3$(aq) (Fig. 4b) can basically be divided into four regions, namely, regions A-B, B-C, C-D, and D-A, and they are paired. That is, the total mass loss within region B-C matches the mass gain within region D-A, while the gain in region A-B is about the same as the loss in region C-D. Furthermore, because these two pairs of regions exhibit opposite trends in mass variation under both scan directions, they are clearly of different origins.

It is known that, because of finite resistance to either reaction direction of a redox couple, the reductive process should always take place, during a potential scan cycle, within a lower potential range than its oxidative counterpart. Accordingly, as indicated in Fig. 4a, only regions B-C and D-A are likely involving redox couple reactions, while regions A-B and C-D are not. As described below, the *m-E* plots in the latter regions bear great similarities to those observed for $Na_2SO_4$(aq).

Figure 5 shows the *m-E* plot for $Na_2SO_4$(aq). The electrode exhibits mass increase with decreasing potential, and vice versa. These trends are the same as those of regions A-B and C-D for $Na_2SO_3$(aq). In addition, the magnitudes of mass variations, ~7 ng for $Na_2SO_4$(aq) and ~10 ng for regions A-B and C-D of $Na_2SO_3$(aq), are also similar. The similarities may suggest that the currents induced under these conditions are of the same origin.

To determine the nature of the redox couple associated with regions B-C and D-A for $Na_2SO_3$(aq) (Fig. 4b), a mass-to-charge ratio (MCR) is defined as

$$\text{MCR} \equiv dm/(dQ/-96500) = -96500(dm/dE)(dE/dt)/I \quad [3]$$

where *dm* is the mass variation (*g*), *dQ* is the charge variation (coulomb), and the remaining quantities are defined as in Eq. 2. *dm*/*dE* is the derivative of the *m-E* plot, while the corresponding current can be obtained from the *I-E* plot (Fig. 4a). MCR, which has a unit of [g/mol $e^-$], has the physical meaning of the mass gain (or loss) caused by reduction (or oxidation) by 1 mol of electron ($e^-$). If the ratio has a positive sign, the species is added onto an electrode upon reduction. This would be the case of a cation intercalation/extraction couple as for either $RuO_2$ or $MnO_2$. In contrast, the ratio has a

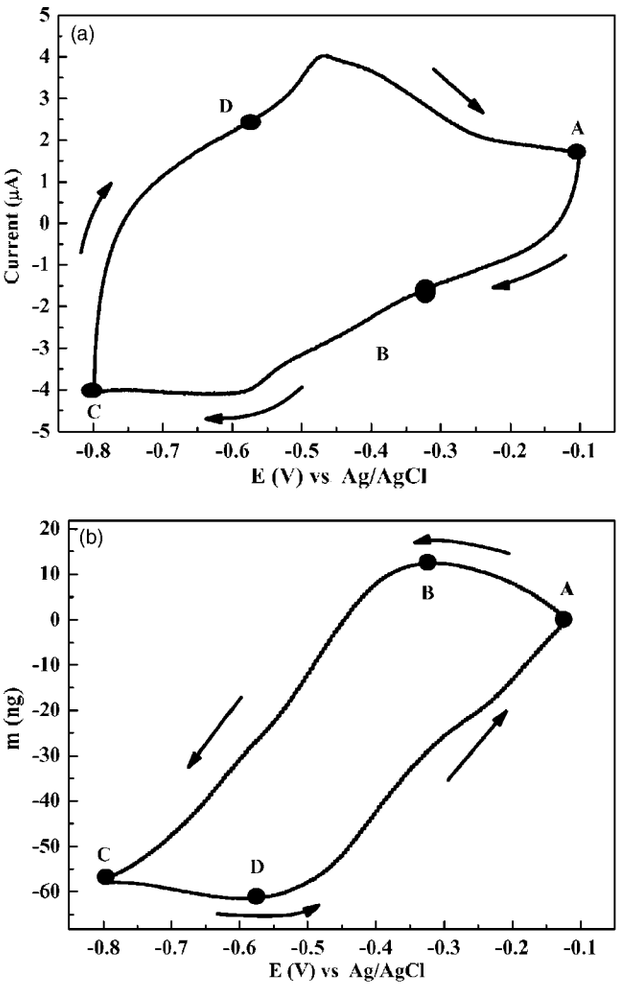


**Figure 4.** Cyclic voltammogram (a) and mass-variation plot (b) of the magnetite electrode in 1.0 M $Na_2SO_3$(aq) at a constant potential scan rate of 2 mV/s. The cycle starts from point A and the arrows indicate the potential scan directions.

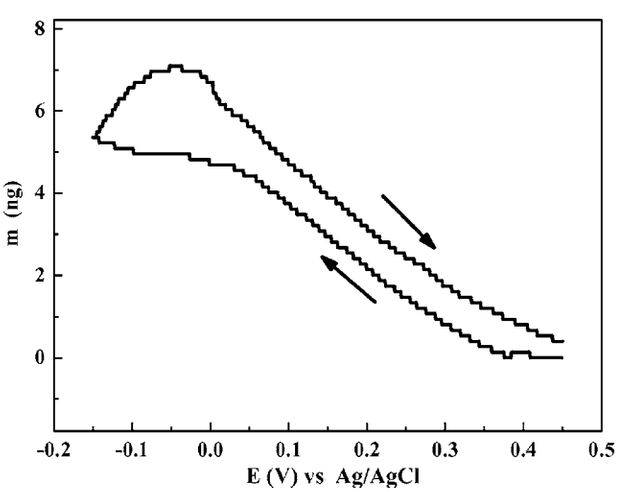


**Figure 5.** Mass-variation plot of the magnetite electrode in 1.0 M $Na_2SO_4$(aq) at a constant potential scan rate of 2 mV/s.

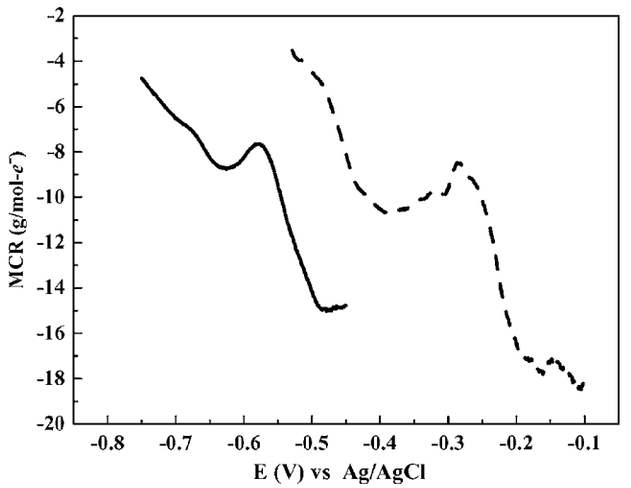


**Figure 6.** Mass-to-charge ratio (MCR) vs potential for the magnetite electrode in 1.0 M $Na_2SO_3$(aq) within region B-C (solid line; reductive scan) and region D-A (dashed line; oxidative scan).

negative sign when the species leaves electrode upon reduction.

Figure 6 shows the MCR-vs-potential (MCR-E) plots for regions B-C and D-A, respectively. Small portions near the reversing potentials of the potential scan, where transitional behavior predominates, are left out for clarity. Three important characteristics are noticed. First, the MCRs are exclusively negative in either regions B-C and D-A. The negative sign suggests that the pseudocapacitive mechanism involved in the present system is completely different from that associated with either $RuO_2$ or $MnO_2$. Second, the MCR exhibits a very broad range of values, which ranges from $-15$ to $-4$ for region B-C and from $-18$ to $-3$ for region D-A. Third, while the MCR in general increases with decreasing potential, the trend is reversed within an intermediate potential range for either region.

*XPS analysis*.— Figure 7a compares the *S* $(2p_{3/2})$ spectra detected by XPS from two electrodes subjected to different conditions. In the first case, the electrode was immersed in 1.0 M $NaSO_3$(aq) for 0.5 h and then rinsed in deionized water. XPS analysis of this electrode detected the presence of S, showing the *S* $(2p_{3/2})$ peak having a center binding energy (B.E.) of 167.5 eV (solid curve). The only possible source of the S signal is the adsorbed $SO_3^{2-}$. For the other electrode (dashed curve), it was first cycled between $-0.2$ and $-0.8$ V in $Na_2SO_3$(aq) for five times and then stopped at $-0.8$ V. XPS analysis of this electrode detected the same *S* $(2p_{3/2})$ peak as that of the first electrode, along with an additional broad shoulder at B.E. = $\sim$ 164 eV. The presence of this redshifted shoulder indicates that a portion of the adsorbed $SO_3^{2-}$ was reduced at $-0.8$ V. There is nevertheless no significant difference for the Fe $(2p_{3/2})$ peak between these two electrodes (Fig. 7b). The redshifted peak was not observed for an electrode that was subjected first to reduction to $-0.8$ V and then to oxidation back to $-0.1$ V. Finally, it is worth mentioning that XPS studies on the electrodes before and after being cycled in the $Na_2SO_4$ electrodes did not detect redshift in the *S* $(2p_{3/2})$ peak.

*Possible reaction mechanisms*.— Table II summarizes a list of electrochemical reactions that involve successive reduction of S, starting from $SO_3^{2-}$ to $S^{2-}$, along with their MCRs. The listing of these reactions by no means implies that the S-containing species adsorbed on the $Fe_3O_4$ surface should exist in exactly the same form as listed. Indeed, the adsorbates might be protonated, and have to coordinate to the surface atoms of the oxide substrate. Nevertheless, the reactions serve to illustrate how the masses of the adsorbates could change as a result of loss of oxygen in response to successive

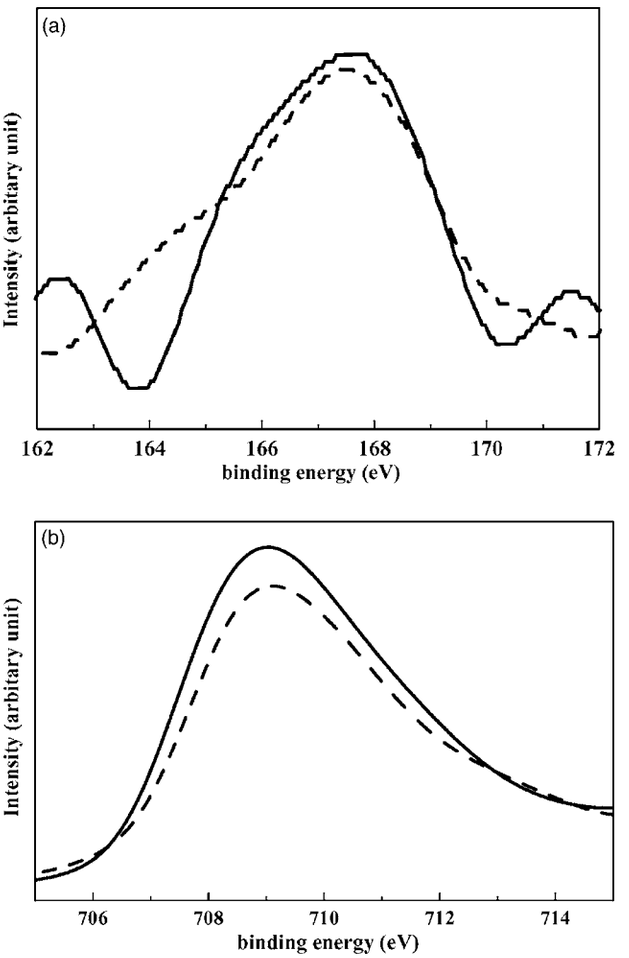


**Figure 7.** The XPS spectra for (a) S $(2p_{3/2})$; and (b) Fe $(2p_{3/2})$. The solid lines are acquired from the electrode after immersion in 1.0 M $Na_2SO_3$(aq) for 0.5 h without potential cycling, and the dashed lines are from the electrode discharged to $-0.8$ V after five cycles.

variations in the valence state of the sulfur element. Protonation and adsorption configuration of the adsorbates will not affect the MCR values of the reactions. Furthermore, it is also apparent that the combination of consecutive reactions in the list will give a net reaction that exhibits an "apparent" MCR of intermediate value. For example, the concurrent occurrence of Reactions 1 (MCR = $-16$) and 2 (MCR = $-8$) in Table II would result in a net reaction

**Table II. Possible reduction reactions for S-containing species.**

| Reaction No. | Reaction | MCR[a] | $E^o$ at pH 10[b] (vs Ag/AgCl) |
|---|---|---|---|
| 1 | $2SO_3^{2-} + 2H_2O + 2e^- \leftrightarrow S_2O_4^{2-} + 4\ OH^-$ | $-16$ | $-0.844$ |
| 2 | $S_2O_4^{2-} + H_2O + 2e^- \leftrightarrow S_2O_3^{2-} + 2\ OH^-$ | $-8$ | $-0.022$ |
| 3 | $S_2O_3^{2-} + 3H_2O + 4e^- \leftrightarrow 2S + 6\ OH^-$ | $-12$ | $-0.617$ |
| 4 | $S + 2e^- \leftrightarrow S^{2-}$ | 0 | $-0.673$ |

[a] MCR denotes the mass-to-charge ratio.
[b] The data have been calculated from Ref. 17.

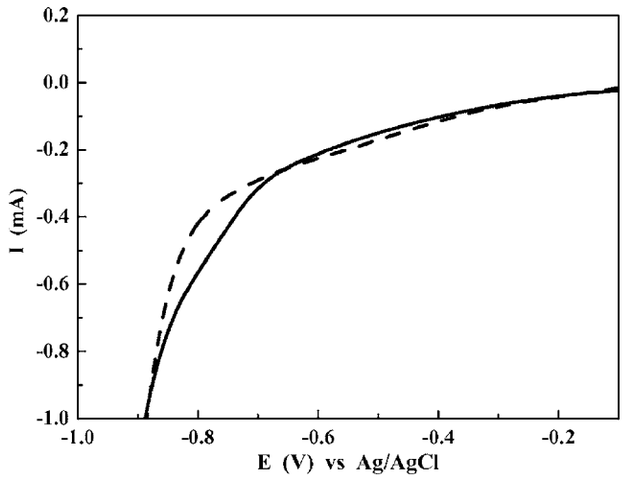


**Figure 8.** Cyclic voltammograms acquired with platinum-foil electrodes in 1.0 M $Na_2SO_3$(aq) (solid line) and 1.0 M $Na_2S_2O_3$(aq) with pH 10 (dashed line). Only the cathodic branch is shown, and the anodic branch basically follows the same curve. The potential scan rate is 2 mV/s.

$$2SO_3^{2-} + 3H_2O + 4e^- \leftrightarrow S_2O_3^{2-} + 6\ OH^-,$$

which has a MCR of −12. Similarly, the combination of Reactions 3 (MCR = −12) and 4 (MCR = 0) gives

$$S_2O_3^{2-} + 3H_2O + 8e^- \leftrightarrow 2S^{2-} + 6\ OH^-$$

with a MCR of −6. Accordingly, the apparent MCR is expected to exhibit a continuous range of values, rather than discrete ones, when there exist continuously variable extents of these reactions.

The reactions listed in Table II have been found to account rather well for the important characteristics exhibited by the MCR-E plots as described earlier. First, these reactions give exclusively negative MCRs, which range from −16 to 0. Second, the theoretical MCR values cover almost the entire range of the observed MCRs for either region B-C or region D-A (Fig. 6). Finally, along the reduction path from Reaction 1 through Reaction 4, the theoretical MCR value first increases, then decreases, and finally increases again. This is consistent with the trend shown in the MCR-E plots (Fig. 6), which show a reverse in the MCR variation trend within an intermediate potential range for either region.

Table II also shows the standard potentials at pH 10 for the listed reactions.[17] For comparison, as shown in Fig. 8, *I-E* plots were also acquired with blank platinum-foil electrodes in 1 M $Na_2SO_3$(aq) and 1 M $Na_2S_2O_3$(aq) with pH 10, respectively. Reaction 1 has the theoretical potential of −0.844 V. The standard potentials of Reactions 2 through 4 are higher than that of Reaction 1. However, consider the fact that the reactant species of Reactions 2 through 4 were not initially present in the electrolyte solution for the $Fe_3O_4$-electrode measurements. They have to be respectively produced from their preceding steps. Therefore, these reactions will automatically be delayed to lower potentials, and each of them should not commence at a higher potential than its preceding step. The standard potentials are related to 1 M of soluble products and the reaction potentials are expected to shift to lower values when the reactant concentrations are less than 1 M.

The standard potentials shown in Table II are for unprotonated anions. In reality, the anions are expected to be mostly in the protonated form in the bulk solution under the present pH condition (pH 10), and the reduction potentials would be different from those shown. The *I-E* profile of a bare platinum electrode in 1 M $Na_2SO_3$(aq) (solid line, Fig. 8) showed an inclined line with increasing reduction current from −0.1 to −0.8 V, below which there was an accelerated current increase due to reduction of $H_2O$. Studies imposing a constant potential with the range between −0.5 and −0.8 V resulted in deposition of sulfur onto the counter electrode. This result indicates that the reduction current within this potential range is due to reduction of sulfite anion to sulfide anion, which was subsequently oxidized to sulfur on the counter electrode. The onset reduction potential, ~−0.1 V, is much higher than the standard potential of Reaction 1, and it may suggest that the protonated sulfite anion is more readily reduced than that indicated in Table II. The *I-E* plot in 1 M $Na_2S_2O_4$(aq) with pH 10 (the dashed line, Fig. 8) is very similar to that of the $Na_2SO_3$(aq) solution, suggesting that protonated $S_2O_4^{2-}$ is also reduced readily within the present potential range.

Taking into account the MCR, potential, and XPS data described above gives strong evidence that the electrode's mass loss observed within region B-C for $Na_2SO_3$ electrolyte solution results from successive reduction of the adsorbed sulfite anions, while the mass gain within region D-A originates from their reverse oxidation counterparts. These redox couples are also responsible for the enhancement of electrochemical capacitance for magnetite in $Na_2SO_3$(aq) solution.

It should be emphasized that the substrate, namely, magnetite, plays an important role in resulting in the pseudocapacitance in $Na_2SO_3$(aq). Indeed, the control study using high surface area (75 $m^2$/g) conducting $SnO_2$,[18] for instance, showed a specific capacitance of 10 F/g-$SnO_2$ in $Na_2SO_3$(aq), which is much smaller than that for magnetite, and can be attributed solely to EDLC. The magnetite substrate could play two roles. First, it provides favorable specific adsorption sites for sulfite anions. As shown in Table I, the extra mass gain during immersion in $Na_2SO_3$(aq) is 852 ng. If this increase is completely ascribed to the adsorption of sulfite anions, it corresponds to adsorption of one sulfite anion out of every 10 Fe ions in the oxide film. Second, the surface adsorption sites of magnetite may have also provided the ideal molecular configuration for $SO_3^{2-}$ to facilitate subsequent redox reactions. That is, the magnetite surface might act as a catalyst for the reactions.

The currents in regions A-B and C-D (Fig. 4a) are instantaneously induced upon the reversal of the potential scan, and they most likely originate from EDLC mechanism. The same mechanism is believed to be operative for the entire applied potential range for $Na_2SO_4$(aq), in view of their similar *m-E* behaviors as described earlier (Fig. 5). During the reductive scan, for example, the current will be the combination of the components resulting, respectively, from diffusion of the adsorbed anions away from the oxide surface or diffusion of cations, namely $Na^+$, toward the surface. The fact of a detected mass increase (region A-B in Fig. 4b and almost the entire reductive scan in Fig. 5) may suggest that the diffusion-in of $Na^+$ predominates. This is reasonable in the sense that $Na^+$ is much lighter and hence diffuses and responses faster than $SO_3^{2-}$.

The average capacitance $C_{avg}$ of region A-B, according to Eq. 1, is about 80 F/g, and the specific surface area of the magnetite film is estimated to be no greater than 83 $m^2$/g, which corresponds to the specific surface area of nonagglomerated crystallites with an average size of 12 nm. This gives magnetite a surface-based specific EDLC of 96 $\mu F/cm^2$ in $Na_2SO_3$(aq). Similarly, a value of ~30 $\mu F/cm^2$ is estimated for $Na_2SO_4$(aq). These specific EDLC values are much greater than those reported for $SnO_2$ and carbon surface, which are nearly 10 $\mu F/cm^2$.[18-20] They, nevertheless, are not exceptional in the systems where specific adsorption of anions takes place.[4] In contrast, the specific capacitance of magnetite in KOH(aq) is estimated to be less than 4 $\mu F/cm^2$. The small capacitance value in KOH(aq) may be caused by oxidation of magnetite surfaces under the highly alkaline condition (pH 14) to form an insulating $Fe_2O_3$ layer. This was indicated by the irreversible oxidation process noticed during the oxidative scan near the high-potential end (Fig. 3).The EQCM plots for KOH(aq) were found to be mostly not reproducible between scans.

## Conclusion

The capacitance mechanisms of a magnetite electrochemical capacitor in $Na_2SO_4$, $Na_2SO_3$, and KOH aqueous solutions have been investigated by EQCM and XPS, along with cyclic voltammetry. Strong specific adsorption of anions was noticed in all solutions. Results indicate that, in the case of $Na_2SO_3$ solution, the capacitive current results from the combination of EDLC and the pseudocapacitance that involves successive reduction of the specifically adsorbed sulfite anions. In $Na_2SO_4$(aq), the capacitive current is due entirely to EDLC. Surface oxidation of the oxide electrode in KOH(aq) results in a significantly low capacitance.

## Acknowledgment

The work is supported by the National Science Council of the Republic of China under contract no. NSC 92-2214-E-002-024.

*National Taiwan University assisted in meeting the publication costs of this article.*

## References

1. B. E. Conway, *J. Electrochem. Soc.*, **138**, 1539 (1991).
2. S. Sarangapani, B. V. Tilak, and C.-P. Chen, *J. Electrochem. Soc.*, **143**, 3791 (1996).
3. D. C. Grahame, *Chem. Rev. (Washington, D.C.)*, **41**, 441 (1947).
4. M. A. V. DeVanathan and B. V. K. S. R. A. Tilak, *Chem. Rev. (Washington, D.C.)*, **65**, 635 (1965).
5. S. Trasatti and G. Buzzanca, *J. Electroanal. Chem. Interfacial Electrochem.*, **29**, App. 1 (1971).
6. L. D. Burke, O. J. Murphy, J. F. O'Neill, and S. Venkatesan, *J. Chem. Soc., Faraday Trans. 1*, **73**, 1659 (1977).
7. B. E. Conway, V. Birss, and J. Wojtowicz, *J. Power Sources*, **66**, 1 (1997).
8. J. P. Zheng and T. R. Jow, *J. Electrochem. Soc.*, **142**, L6 (1995).
9. J. P. Zheng and T. R. Zheng, *J. Electrochem. Soc.*, **145**, 49 (1998).
10. H. Y. Lee and J. B. Goodenough, *J. Solid State Chem.*, **144**, 220 (1999).
11. H. Y. Lee and J. B. Goodenough, *J. Solid State Chem.*, **148**, 81 (1999).
12. N. L. Wu, Y. P. Lan, C. Y. Han, S. Y. Wang, and L. R. Shiue, in *Electrochemical Capacitor and Hybrid Power Sources*, R. J. Brodd, D. H. Doughty, J. H. Kim, M. Morita, K. Naoi, G. Nagasubramanian, and C. Nanjundiah, Editors, PV 2002–7, p. 95, The Electrochemical Society Proceedings Series, Pennington, NJ (2002).
13. N. L. Wu, S. Y. Wang, C. Y. Han, D. S. Wu, and L. R. Shiue, *J. Power Sources*, **113**, 173 (2003).
14. S. Y. Wang and N. L. Wu, *J. Appl. Electrochem.*, **33**, 345 (2003).
15. L. R. Shiue, N. L. Wu, D. S. Wu, C. W. Chao, and Y. P. Lan, U.S. Pat. 6,678,147 (2004).
16. T. Brousse and D. Bélanger, *Electrochem. Solid-State Lett.*, **6**, A244 (2003).
17. *Handbook of Chemistry and Physics*, 83rd ed., pp. 8-21–31, D. R. Lide, Editor, CRC Press, Boca Raton, FL (2002).
18. N. L. Wu, C. Y. Han, and S. L. Kuo, *J. Power Sources*, **109**, 418 (2002).
19. G. Salitra, A. Soffer, L. Eliad, Y. Cohen, and D. Aurbach, *J. Electrochem. Soc.*, **147**, 2486 (2000).
20. N. L. Wu and S. Y. Wang, *J. Power Sources*, **110**, 233 (2002).